Smart Structures and Systems, *Vol. 33*, *No. 3* (*2024*) *227-241*
https://doi.org/10.12989/sss.2024.33.3.227

Real-time online damage localisation using vibration measurements of structures under variable environmental conditions

K. Lakshmi*

CSIR-Structural Engineering Research Centre, *CSIR Campus*, *Taramani*, *Chennai-600113*, *Tamilnadu*, *India*

(*Received June 20*, *2023*, *Revised November 22*, *2023*, *Accepted January 29*, *2024*)

Abstract. Safety and structural integrity of civil structures, like bridges and buildings, can be substantially enhanced by employing appropriate structural health monitoring (SHM) techniques for timely diagnosis of incipient damages. The information gathered from health monitoring of important infrastructure helps in making informed decisions on their maintenance. This ensures smooth, uninterrupted operation of the civil infrastructure and also cuts down the overall maintenance cost. With an early warning system, SHM can protect human life during major structural failures. A real-time online damage localization technique is proposed using only the vibration measurements in this paper. The concept of the 'Degree of Scatter' (DoS) of the vibration measurements is used to generate a spatial profile, and fractal dimension theory is used for damage detection and localization in the proposed two-phase algorithm. Further, it ensures robustness against environmental and operational variability (EoV). The proposed method works only with output-only responses and does not require correlated finite element models. Investigations are carried out to test the presented algorithm, using the synthetic data generated from a simply supported beam, a 25-storey shear building model, and also experimental data obtained from the lab-level experiments on a steel I-beam and a ten-storey framed structure. The investigations suggest that the proposed damage localization algorithm is capable of isolating the influence of the confounding factors associated with EoV while detecting and localizing damage even with noisy measurements.

Keywords: damage localization; environmental and operational variability; fractal dimension; laboratory framed structure; model-free SHM; shear building

1. Introduction

Civil infrastructure is often made to last for a long time, sometimes even a century. During their long service period, structural degradation is bound to take place due to aging, unanticipated loads, fatigue, corrosion, etc., and sometimes may even collapse during their operation due to rapid deterioration. Therefore, a reliable way of keeping track of this progressive deterioration in the infrastructure is essential to ensure the users' safety and make informed decisions about the maintenance schedule to improve their longevity. In the recent past, structural health monitoring (SHM) has evolved as the most promising technology for the real-time diagnosis of structures. Based on these timely diagnoses, the safety of these structures can be ensured through timely, effective maintenance schedules at reduced costs.

Recent advancements in sensor technologies, high-speed data acquisition systems, and the availability of low-cost, ubiquitous sensors, apart from advancements in data/signal processing techniques, have immensely contributed to the rapid strides of SHM technology. Structural damage diagnosis is the core element of SHM, and several algorithms for damage diagnosis are reported in the literature. Several well-organized review papers in the literature discuss some of these methodologies (Avci *et al*. 2021, An *et al*.2019, Das and Roy 2022).

Environmental and operational variability (EoV) often poses a greater challenge for engineering structures. EoV influences the measured structural responses even in a healthy structure. Unless the issues related to EoV are comprehensively addressed while devising the damage diagnostic algorithms, problems like false positive or negative detections may often take place during health monitoring. Therefore, EoV is one of the most significant issues to handle while detecting damage to civil infrastructures in real-time SHM applications.

Damage identification techniques developed using measured dynamic responses are quite popular for damage detection, localization, and estimating its severity. The premise behind these techniques is that modal characteristics like frequency and mode shape are functions of structural physical attributes like mass, damping, and stiffness. These modal characteristics will vary when there is a change in the physical attributes due to structural damage. These techniques are theoretically sound. However, modal parameter identification of practical spatially large engineering structures needs a large number of sensors, and extracting a large number of modes, which is a prerequisite for damage diagnosis, is also not feasible from ambient vibrations. In view of this, the modal-based diagnostic techniques are rather practically difficult to use

*Corresponding author, Ph.D.,
E-mail: lakshmik@serc.res.in

ISSN: 1738-1584 (Print), 1738-1991 (Online)

on real structures. Other difficulties associated with modal-based techniques include sensitivity to measurement noise, low sensitivity to minor incipient damages in the structure, and handling EoV is rather difficult. Due to all these practical constraints of modal-based methodologies, signal processing-based damage diagnosis techniques have recently gained popularity as they are scalable to practical engineering structures. Widely used signal processing-based damage diagnostic techniques are multivariate analysis (Rao *et al*. 2015, Kumar *et al*. 2020, Zhang *et al*. 2021, Cao *et al*. 2022, Hao *et al*. 2022), time series (Lakshmi and Rama Mohan Rao 2018b, Entezami *et al*. 2020, Do and Gül 2020, Bernagozzi *et al*. 2021, Chegeni *et al*. 2022), time scale (Sanchez *et al*. 2020, Katunin *et al*. 2021), time-frequency methods (Rama Mohan Rao and Lakshmi 2015, Wang *et al*. 2022), special techniques to handle EoV (Lakshmi 2021, Sarmadi *et al*. 2021, Torzoni *et al*. 2022, Huang *et al*. 2023), multi-model techniques (Lakshmi and Rama Mohan Rao 2018a, Lakshmi and Rama Mohan Rao 2019, Lakshmi 2020), inverse algorithms (Rama Mohan Rao *et al*. 2015, Lakshmi and Rama Mohan Rao 2019, Shallan and Hamdy 2022, Beygzadeh *et al*. 2022), computer vision (Liu *et al*. 2023), and artificial intelligence/ machine learning (Avci *et al*. 2021, Guo *et al*. 2022, Wang *et al*. 2022).

In a nutshell, any practically amenable damage detection algorithm for civil infrastructure should be applicable for online SHM with rapid damage assessment features, should work without correlated finite element models with limited instrumentation requirements, and should be capable of handling EoV. Finally, they should be capable of assessing the state of the structure with only measured output responses.

In view of these, a rapid damage assessment technique amenable to online SHM and capable of handling EoV is presented in this paper. The fractal theory is used for localizing the damage. A new damage localization index that can properly handle EoV is proposed. The suggested method's efficiency is evaluated numerically and experimentally through lab-level experiments using beam as well as framed structures. The investigations carried out on the damage detection algorithm discussed in this paper suggest that it is simple, accurate, and capable of handling EoV and measurement noise.

2. Theoretical background

The proposed algorithm makes use of the scatter in the vibration measurements of each sensor placed on the structure. Accordingly, the '*Degree of Scatter*' (DoS), which is a prime component in the proposed damage localization algorithm, is evaluated at each sensor node and is defined as the amount of scattering of the measured acceleration time history at any typical node from its mean value. The '*Degree of Scatter*' can be calculated from the discrete-time history measurements $\ddot{z}_s = [\ddot{z}_s(1), \ddot{z}_s(2), \ddot{z}_s(3), \ldots . \ddot{z}_s(N)]$ at any typical sensor node S as

$$\Delta_s(\ddot{z}) = \log(\text{variance}\ (\ddot{z}_s)) \quad (1)$$

where Δ_s is the calculated '*Degree of Scatter*' at any typical sensor node, s, and the data points in the measured response are denoted by N. Eq. (1) can be used as a measure to identify how far a set of numbers (acceleration data) is from its mean value. The greater the value Δ_s, the higher the scattering of the sampling points (acceleration) from their mean value. Since this value is likely to vary with the size of the acceleration time history vector, it is necessary to keep the size constant while comparing the time history responses before and after the damage to get meaningful information about the presence of damage. Once all the points related to the '*Degree of Scatter*' are evaluated at each measured sensor node, these points can be connected to form a waveform, which is referred to as the degree of scatter waveform or simply DoSWF. The logarithm is used in Eq. (1) to make the waveforms independent of excitation amplitude on the structure during pristine (healthy structure) and current measurements with a possible presence of damage.

2.1 Localisation of damage

It is possible to think of the DoSWF as a two-dimensional waveform. Fractal theory (Katz 1988) can be used to quantify the complexity of the DoSWF and identify waveform (WF) changes caused by either localized damage or EoV.

Along the DoSWF-associated spatial waveform, a moving, overlapping window with a fixed length is traversed. At least three sampling points must be included for each moving window, with the middle of the window coinciding with the middle sampling point. A sensor mounted on the structure corresponds to each sampling point in the DoSWF. The Fractal Dimension value is estimated using the DoSWF values associated with the three sampling points in a typical window, and it is assigned to the spatial sensor located at the mid-sampling point. Similarly, the window is shifted along DoSWF, point by point, covering each location of the spatial sensor. Any localized damage manifests as complexity in the DoSWF, which causes a sensor placed close to the complexity in the WF to register a relatively large magnitude of Fractal Dimension value. Therefore, the high Fractal Dimension value of any sensor can be used to localize the damage. However, EoV also affects the DoSWF, and the Fractal Dimension estimate can pick up these changes quite precisely. Katz's fractal dimension (KFRCD) (Katz 1988) is perhaps the most appealing Fractal Dimension estimation among those reported in the literature (Katz 1988, Higuchi 1988, Normant and Tricot 1991, Esteller *et al*. 1999, Paramanathan and Uthayakumar 2008) because of its straightforward idea, ease of computer implementation, and reduced sensitivity to noise.

Any typical waveform can be thought of as a collection of m sampling points $wf = [wf_1, wf_2, wf_3, \ldots . wf_m]$. The x and y coordinates of any sampling point, i, on the DoSWF are $wf_i = (x_i, y_i)$. With this, for any typical spatial location, x_i on DoSWF, Katz's Fractal dimension (KFRCD) can be calculated as

$$KFRCD_n(x_i) = \frac{\log_{10}(n)}{\log_{10}\left(\frac{d(x_i)}{L(x_i)}\right) + \log_{10}(n)} \quad (2)$$

where n refers to the number of waveform sampling intervals covered within any typical moving window. This number (n) will usually be 2. However, it can be even more than 2. The total distance from the starting sampling point to the end sampling point of any typical moving window is $L(x_i)$ and can be written as $L(x_i) = \sum_{i=1}^{n} \|wf_{i+1} - wf_i\|$. $d(x_i)$ refers to the maximum length of the waveform from the starting sampling point x_1 to the current sampling point, x_i on the waveform. It can be written as

$$d(x_i) = \max[\text{dist}(x_1, x_i)] \quad (3)$$

For identifying damage, the KFRCD given in Eq. (2) can effectively handle simple wave profiles with very regular shapes. Its efficacy cannot be assured when applied to more intricate waveforms. In view of this, it is decided to use a more advanced version of KFRCD (Li *et al*. 2011), which can work for complex wave profiles. In this version, the Fractal Dimension is defined using the included angle α_j created by the tangents drawn on the DoSWF from the moving window's start and end positions. The subscript j stands for the moving window number from the left.

$$\alpha_j(x_i) = \pi - \arccos\left(1 - 2\left[0.5 \times 10^{\frac{log_{10}(2)}{KFRCD_2(x_i)}}\right]^2\right) \quad (4)$$

The FRCD, considering the included angles, can be written as

$$FRCD(x_i) = \frac{\alpha_j(x_i) - \alpha_j(x_{i-1})}{(x_i - x_{i-1})} = \frac{\left\{arccos\left(1 - 2\left[0.5x10^{\frac{log_{10}(2)}{KFRCD_2(x_{i-1})}}\right]^2\right) - arccos\left(1 - 2\left[0.5x10^{\frac{log_{10}(2)}{KFRCD_2(x_i)}}\right]^2\right)\right\}}{H} \quad (5)$$

where h is the horizontal distance between two successive sampling points.

The difference in the evaluated damage feature, $\Delta FRCD$, of the DoSWF associated with two different sets of dynamic time history data of the structure at any spatial location x_i, can be written as

$$\Delta FRCD_{p,\,q}(x_i) = \text{abs}(\text{FRCD}^p(x_i) - \text{FRCD}^q(x_i)) \quad (6)$$

where p and q refer to the features extracted from two entirely different dynamic time history dataset numbers and x_i refer to the spatial location (sensor location) on the structure where the fractal dimension is resolved. Referring to the data compiled at two different time instants and are the features extracted from two entirely different sets of dynamic time history data measured at the same time/day or at a separate time/day. The damage can be localized based on the higher magnitude of the Fractal Dimension at any spatial location.

3. Proposed algorithm

There are two phases in the proposed algorithm for damage detection. The first phase is referred to as 'Training', while the second phase is referred to as 'Execution'.

3.1 Training

The training component of the algorithm works on the vibration responses compiled from the healthy structure and can even work in offline mode. The residual features shown in Eq. (6) are recovered from the dynamic responses measured using the accelerometers placed at distinct spatial locations on the healthy structure. In general, the vibration measurements are expected to have confounding effects related to EoV. These residual damage features are utilized to create the thresholds for each sensor location in this phase. In order to handle the effect of EoV, these established threshold limits using the dynamic responses measured on the pristine structure are used in the diagnosis phase to assess whether the current state of the structure is healthy or damaged.

The key activity of this phase of the algorithm is to compile the vibration responses from the structure measured under several realistic scenarios of variable operating and environmental conditions in different time zones of the day throughout the year. To improve the accuracy of the damage diagnosis, it is desirable to compile the measured vibration data covering all the possible diverse practical scenarios. The compiled time history data is divided into small data-segments. Each of the several such data-segments compiled has the same number of data samples and should not be less than 1000 samples.

The details of the algorithm to determine the threshold limits are given below:

i. To incorporate all the potential variations, the dynamic response (acceleration) of the targeted (instrumented) structure is acquired under various operating and environmental conditions. A large number of datasets of such time history measurements encompassing all possible variable conditions certainly improve the accuracy of the detection.
ii. The measured dynamic response from all the sensors placed on the structure in a given instance is divided into many segments such that each segment contains samples not less than 1000. Depending on the sampling frequency and the duration of the measurement, at a specific instance, each segment of data may include even more samples. However, it is to ensure that the number of samples in each segment is the same. These partitioned segments of data formed for all the measured dynamic responses

at different instants of time/day are named "DS-1", "DS-2",..., and "DS-m", where m refers to the total number of segments formed.

iii. Using the DS-1, the DoS at all N_s sensor nodes is evaluated using Eq. (1). The nodal ordinates associated with DoS are connected to create DoSWF for DS-1. Perform fractal dimension analysis on the waveform related to DS-1, and compute FRCD(s,1), s = 1 to N_s; using Eq. (5).

iv. Repeat step(iii), each time using a different data-segment, i.e., DS-2, DS-3,…DS-m to compile the FRCD matrix, (FRCD(s, k), s = 1 to N_s; k = 1 to m).

v. Compute the difference between the FRCD values of DS-1 and 'DS-2, corresponding to each sensor location, s, as $\Delta FRCD_{12}(s) = \text{abs}(\text{FRCD}^1(\text{s},1) - \text{FRCD}^2(\text{s},2))$.

vi. Step(v) is repeated by comparing DS-1 each time with a different segment from the available (m-2) segments in the baseline pool (i.e., leaving DS-2) and retrieving the FRCD feature differences for each combination $\Delta FRCD_{1q}(s)$, s = 1 to N_s; q = 3 to m.

vii. In this way, each segment produces [m-1] combinations, resulting in [m -1] numbers of $\Delta FRCD$ values, $\Delta FRCD_{p,q}(s)$, s = 1 to N_s. The subscripts p and q belong to two unique segments.

viii. The threshold limit THL(s) for each sensor node is determined as follows.

$$THL(s) = \left[\text{mean}\left(\Delta FRCD(s)\right) + 3 \times \left(\text{standard deviation}\left(\Delta FRCD(s)\right)\right)\right] \quad (7)$$

These threshold limits are established by assuming that these $\Delta FRCD$ values are normally distributed.

ix. The THL vector is used in the second phase, to compute damage localization indices (DLIs).

3.2 Execution phase

This phase of the algorithm assesses the structure's present (unknown) state. This phase can completely run online. The various steps associated with this phase are as follows.

i. The measured acceleration responses of the targeted structure in its present (unknown) state are compiled. These compiled data are divided into several data-segments to form the current pool of data-segments as was done in the case of the baseline pool during the training phase. It should be ensured that the number of samples per segment is the same as in the baseline pool.

ii. The FRCD feature difference at each sensor node s can be evaluated by combining each data-segment of the current pool with any arbitrarily chosen baseline pool data-segment of the structure, $\Delta FRCD_{c,\,b}(s)$; s = 1 to N_s. The subscripts c and b refer to the current and baseline pool, respectively.

iii. For each sensor node, the damage localization index (DLI) is calculated using the FRCD feature difference calculated in step(ii) and the THL vector evaluated in the training phase of the proposed algorithm.

$$DLI(s) = \Delta\text{FRCD}_{c,\,\text{b}}(s) - THL(s) \quad (8)$$

$$\text{Time of Damage Incipience } (TDI) = C \times SF/NSMP \quad (9)$$

where C is the earliest current data-segment number with positive DLIs, SF is the sampling frequency, and NSMP refers to the samples per data-segment. When the structure is in good condition, the normalized damage feature difference, $\Delta FRCD^s_{c,r}$, will be within the threshold limits THL(s) at all sensor nodes. When the structure has damage, the sensors located closest to the damage will show positive DLIs, while the remaining DLIs will be either zero or negative. Therefore, the damage in the structure will be present in the vicinity of the sensor(s) whose DLIs are positive. TDI can be determined using Eq. (9).

The flow chart corresponding to the two phases of the proposed damage diagnostic algorithm is shown in Fig. 1. In the next section, studies carried out using synthetic data for numerical evaluation as well as measured responses from lab-level experiments for experimental evaluation of the damage diagnostic technique, are described.

4. Numerical simulations

The performance of the suggested DOS-based algorithm has been verified through numerical simulation tests using two numerical examples. The first one is a simply supported beam. It is considered a first example as medium-range bridges are usually idealized as simply supported beams for damage detection as it is the prime load-carrying member. A 25-storey tall framed structure modeled as a shear building is the second example considered to test the proposed algorithm. EOV is simulated in numerical studies to test its resilience against such confounding factors. For all the numerical studies considered here, noise is added to the computed responses to test the influence of noise on the algorithm's detection ability.

4.1 Simply supported beam

A simply supported beam with cross-sectional dimensions of 0.45 m × 0.5 m and a span of 6 m is considered. The beam and its properties are shown in Fig. 2. Even though there are 25 elements and 24 active nodes in the finite element (FE) discretization of the beam, the dynamic response from only 12 equidistant nodes is used in the present simulation to imitate an experiment with only 12 sensors placed on the structure. The first four frequencies are found to be 32 Hz, 127 Hz, 286 Hz, and 509 Hz. Rayleigh damping is employed in the numerical simulations with 1.5% for the first two modes. Band-limited white Gaussian noise is used to excite the structure. The Newmark-beta algorithm is used to compute dynamic responses. The sampling rate is 1000 Hz and it works out to a time step length of 0.001 sec.

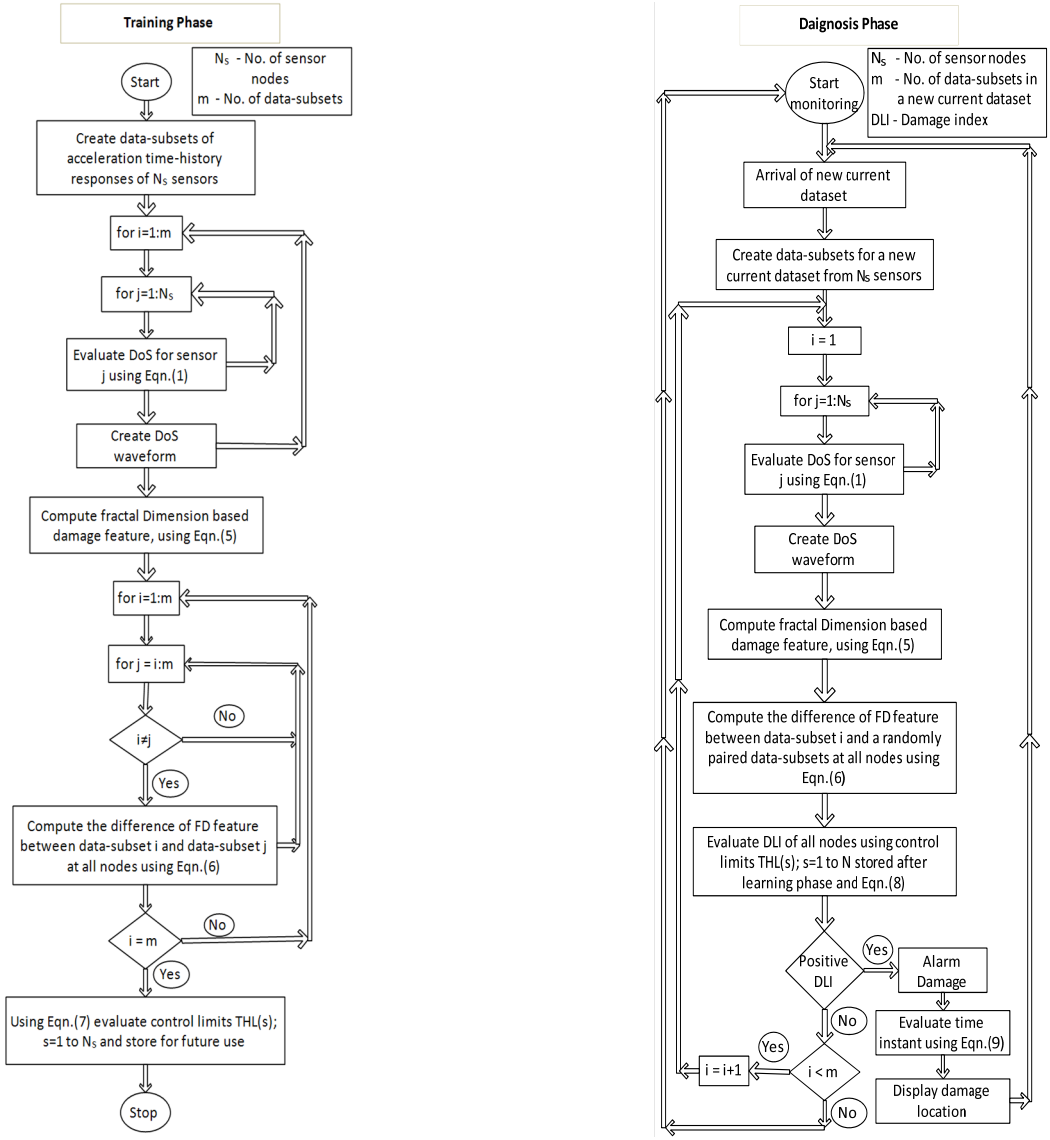

(a) Training phase (b) Diagnosis phase

Fig. 1 Flow chart of the proposed damage localization algorithm

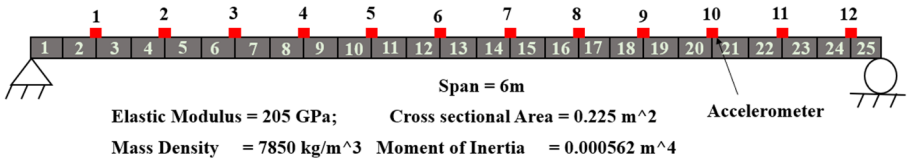

Fig. 2 Simply Supported beam- Element numbers are indicated in white font within the elements and sensor numbers in black font

The same FE model of the beam is used to perform 600 sets of dynamic simulations, each time with a different excitation amplitude, to simulate operational variability. Similarly, varying the temperature randomly between -10°C to +45°C during the FE analyses while computing the dynamic responses of the beam simulates environmental variations. Changes in the modulus of Elasticity of the RCC beam due to temperature variations are considered as per the curve (Yan *et al*. 2005) shown in Fig. 3.

During field experiments, measured acceleration time history responses are corrupted by the measurement noise. Therefore, to simulate practical situations, white noise is added to the computed dynamic responses. To generate noise-polluted vibration responses, normally distributed random noise is added to the dynamic responses as

$$\ddot{z}_m = \ddot{z} + \zeta.\,\mathrm{std}(\ddot{z}).randn \qquad (10)$$

where $\ddot{z}_m$ and $\ddot{z}$ are the noise-polluted and the noise-free

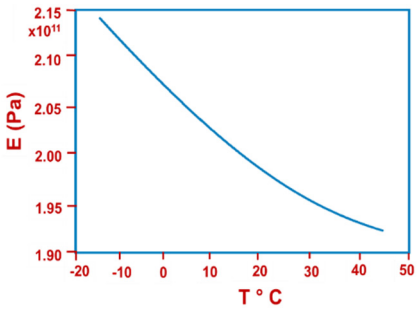

Fig. 3 Young modulus of steel with varying temperature (Yan *et al*. 2005)

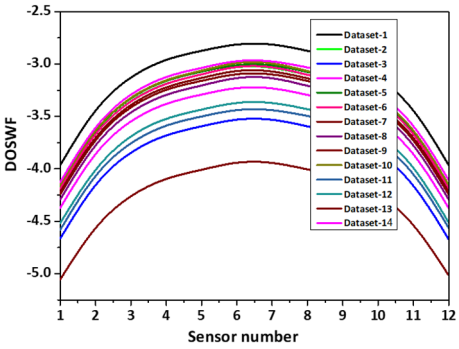

Fig. 4 DoSWF values evaluated for some typical datasets of the Simply Supported beam in healthy state considering EoV

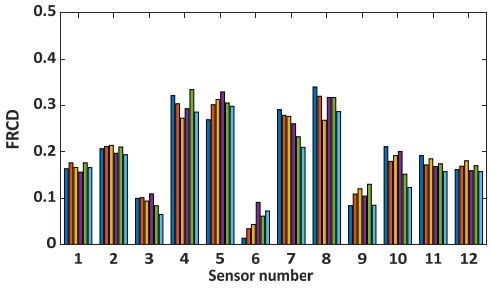

Fig. 5 Fractal dimension (FRCD) values evaluated for some typical waveforms (DoSWF) of the Simply Supported beam in healthy state considering EoV

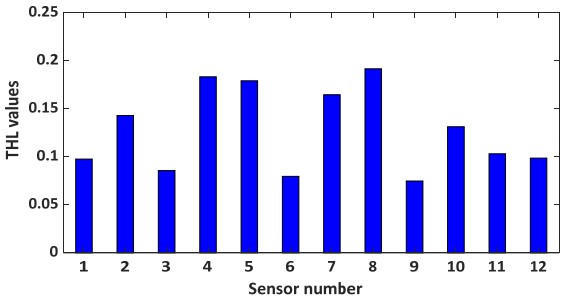

Fig. 6 Threshold limits (THL values) of each sensor evaluated for the Simply Supported healthy beam

computed acceleration time history responses, respectively; z is the noise percentage, and *randn* is a normal distribution vector with zero mean and unit standard deviation. Random noise levels of 2% and 4% are taken into account in the numerical investigations presented in this paper. Furthermore, due to the uncorrelated noise sequences affecting distinct nodes, a harsh experimental scenario is simulated.

Six hundred datasets of vibration responses are collected from six hundred independent FE simulations of the healthy structure with EoV, as discussed earlier. Each of these datasets is partitioned into two segments of 1000 samples each. These 1200 data-segments form the baseline pool training the algorithm. Eq. (7) is used to arrive at the threshold limits (THL) for each sensor location.

The waveforms DoSWF shown in Eq. (1) are evaluated using the acceleration time history response datasets of the healthy structure with varied operational and environmental (EoV) conditions. DoSWF values evaluated for typical healthy data segments of the structure are illustrated in Fig. 4. Using these waveforms, the fractal dimension, i.e., FRCD values, are evaluated using Eq. (5). Fig. 5 illustrates the FRCD values of some typical waveforms of the structure. Subsequently, the $\Delta FRCD$ values are evaluated using steps (v) to (vii) of the proposed training phase of the diagnosis algorithm presented in section 3. Using all $\Delta FRCD$ values for all the data segments of the healthy structure, the threshold limits, i.e., THL values are determined using Eq. (7) for all the sensor nodes on the structure. The THL values evaluated for the simply supported beam are shown in Fig. 6.

The stiffness of element-10 is reduced by 10%, and similarly, element-20 by 8% to artificially simulate damage in the numerical model of the beam. It is assumed that the beam is damage-free for the first six seconds of the simulations and subsequently undergoes damage. Accordingly, the acceleration time history responses are evaluated using the FE model of the beam. Therefore, the first six data segments (of 1000 samples each) are for damage-free beams, and the remaining corresponds to the structure with multiple damages. All the dynamic FE simulations are carried out by considering EoV. Such simulations carried out with varying operational and environmental loads clearly test the ability of the proposed damage localization index (DLI) to localize the damage in the structure under the influence of EoV. The data-segments compiled from these simulations form the current data pool and are used to arrive at the THL vector. This THL vector is subsequently used to evaluate the DLIs during the next phase.

Eq. (8) is used to compute DLIs for each sensor location. Figs. 7 and 8 show the computed DLIs for noise-free and noisy data, respectively. It can be noted from Figs. 7 and 8 that the positive DLIs clearly reflect the presence of damage in the beam. It can be concluded from the plot shown in Fig. 7(a) without any positive DLI that the beam is damage-free. The DLIs shown in Fig. 7(a) are for the healthy beam (6^{th} data segment). It is evident from this study that the suggested diagnostic algorithm has accurately captured the damage-free state of the beam and is not influenced by the EoV, which may perhaps drive a false positive diagnosis. Similarly, it is discovered that the DLIs for the fifth and tenth sensor nodes in Fig. 7(b) are positive,

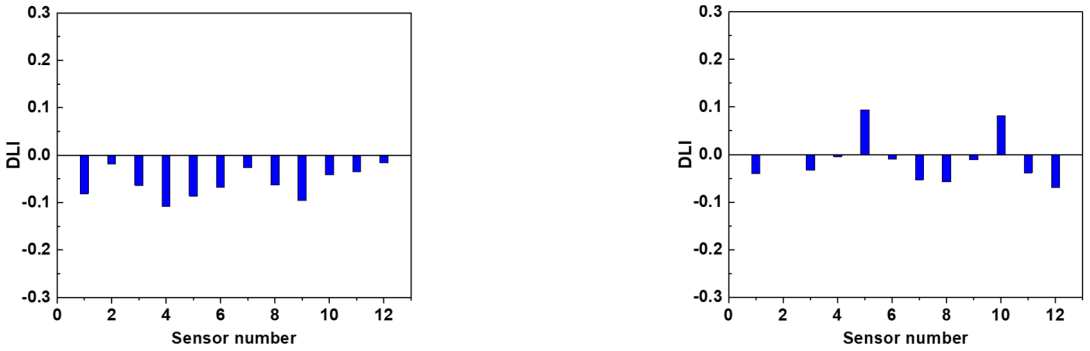

(a) 6th data-segment (b) 7th data-segment

Fig. 7 Detection of damage in Simply supported beam with noise-free measurements

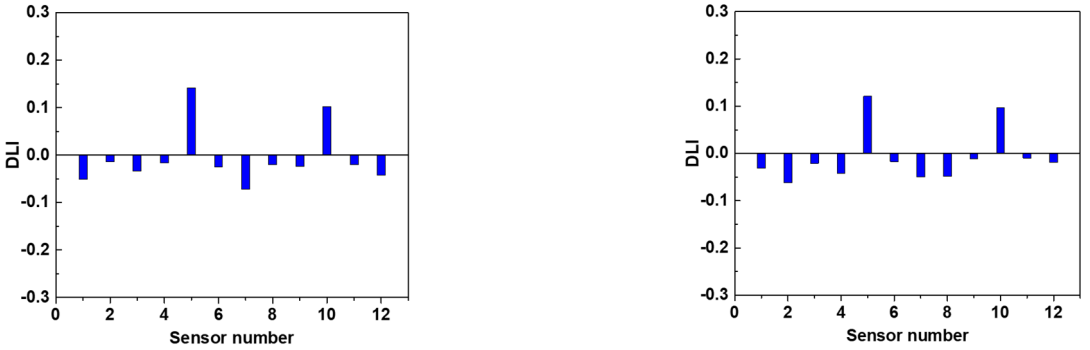

(a) 7th data-segment - 2% noise (b) 7thdata-segment - 4% noise

Fig. 8 Detection of damage in simply supported beam with noisy measurements

whereas the DLIs for the others are negative. The sensor nodes, in this case, display positive DLIs closest to the 10th and 20th elements of the beam, where damage is currently being simulated. The results of this experiment show that the suggested diagnostic algorithm can locate the damage rather precisely while taking into account confounding variables like EoV. Eq. (9) is used to calculate the precise TDI, and it is worked out to be 6 seconds. The execution phase of the proposed technique, which involves extracting damage features from the current responses of 12 sensor nodes, takes 0.73 seconds to complete.

The results of similar investigations employing noisy data from data-segment 7, are presented in Fig. 8 for various noise levels. It is evident from Fig. 8 that the damage can be localized even in the presence of noise from the positive DLIs.

4.2 Twenty-five-storey frame structure

The second numerical example considered is a shear building model of a 25-storey frame structure, shown in Fig. 9. The properties of the shear building are shown in Table 1. The shear building is excited at the 25th floor using random load. Newmark-beta time marching scheme is employed with a time step length of 0.001 (i.e., sampling frequency: 1000 Hz) for dynamic analysis of the structure with Rayleigh damping. The damping is considered as 1.5% for the first two modes. Both noise-free and noisy vibration data are used in the investigations, just like the earlier numerical simulations.

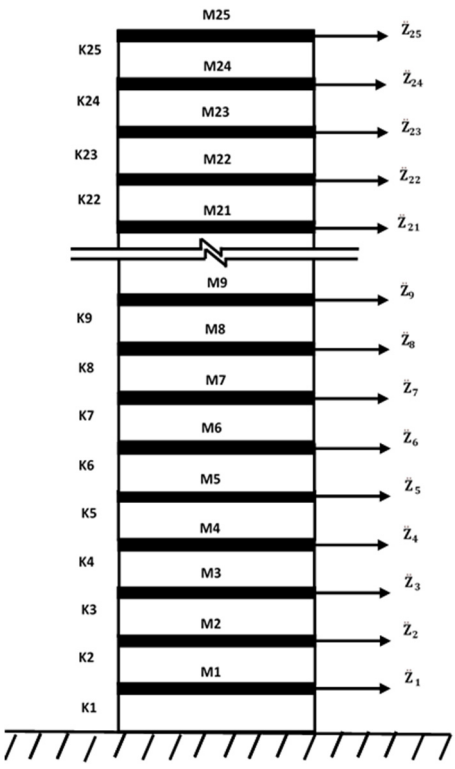

Fig. 9 25-storey shear building model

Table 1 Storey stiffness, storey mass, and natural frequencies of the 25 storey shear building

	Stiffness (KN/m)	Floor mass (Kg)
Bottom 15 stories	4000	2500
Top ten floors	3000	2000
Natural frequencies (Hz)	1.201, 3.599, 5.983, 8.344, 10.674, 12.963, 15.203 and 17.386	

By changing the amplitudes of random excitation periodically, 600 sets of dynamic simulations are performed using the same numerical model. Throughout the finite element simulations, the temperature is also randomly adjusted between -10°C to +45°C. Changes in the Young's Modulus of the steel structure as a result of temperature fluctuations, shown in Fig. 3, are taken into account during the FE simulations.

Each simulation is run for two seconds to compile two thousand samples for the baseline pool. The baseline pool is created by partitioning the time history data into several data-segments of 1000 samples each. The algorithm's training phase is used to evaluate the threshold limit for each sensor location.

The storey stiffness of the 6th, 14th, and 22nd storey of the 25-storey shear building is reduced by 8%, 10%, and 6%, respectively, to numerically simulate multiple damages in the structure. The structure is assumed to be initially healthy during the simulations and to have suffered damage after nine seconds. Accordingly, the current pool is created by appending nine data-segments (each with 1000 samples), from the baseline pool, and the rest of the current pool consists of current data-segments formed from the simulations carried out shear building model with single and multiple damages. EoV is considered all through these simulations.

The DLIs are evaluated using Eq. (8) and presented in Fig. 10, with noise-free measurements. On similar lines, Fig. 11 presents the DLIs for some specific data-segments with noise. The DLIs for the seventh data-segment shown in Fig. 10(a), are for the frame structure in a healthy state. It can be easily verified from Fig. 10(a) that the suggested method properly identified the structure's healthy state. It can be observed from Fig. 10(b) that the DLIs are positive only for the fifth, sixth, thirteenth, fourteenth, twenty-first, and twenty-second sensor nodes. It indicates that the damage locations in the structure are in the vicinity of the sensor nodes with positive DLIs. Since the damage is simulated in the shear building's 6th storey (represented by the 5th and 6th sensor nodes), 14th storey (represented by the 13th and 14th sensor nodes), and 22nd storey (represented by the 21st and 22nd sensor nodes) during FE analysis, the corresponding sensor nodes exhibit positive DLIs. This numerical experiment demonstrates unequivocally that the suggested damage diagnostic approach is efficient in managing EoV while localizing the various structural damages. The precise time of damage incipience (TDI) is 9 seconds.

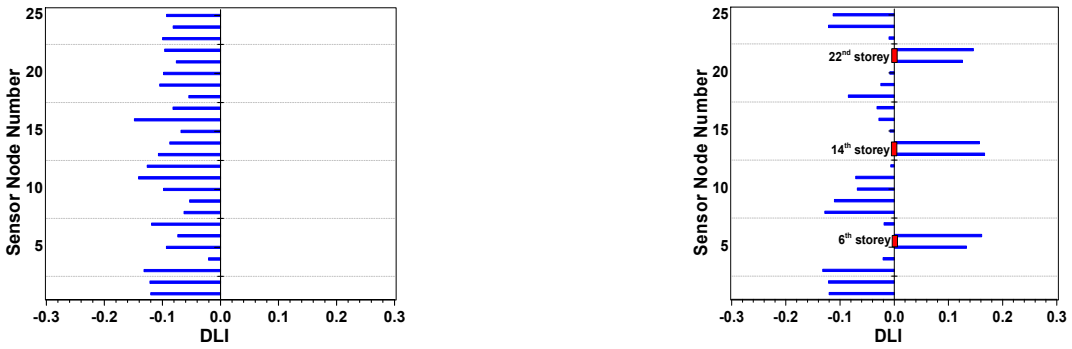

(a) 9th data-segment (b) 10th data-segment

Fig. 10 DLIs for the 25-storey shear building with noise-free measurements

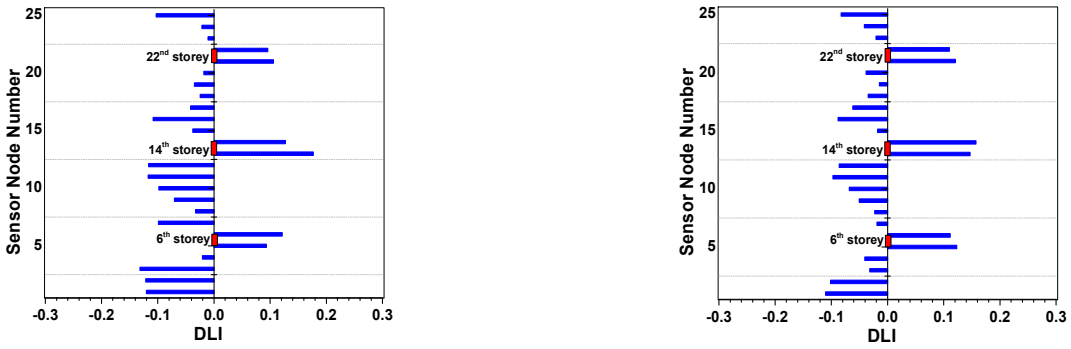

(a) Noise-2% (b) Noise-4%

Fig. 11 DLIs of the 25-storey shear building with the noisy response: Data-segment-10

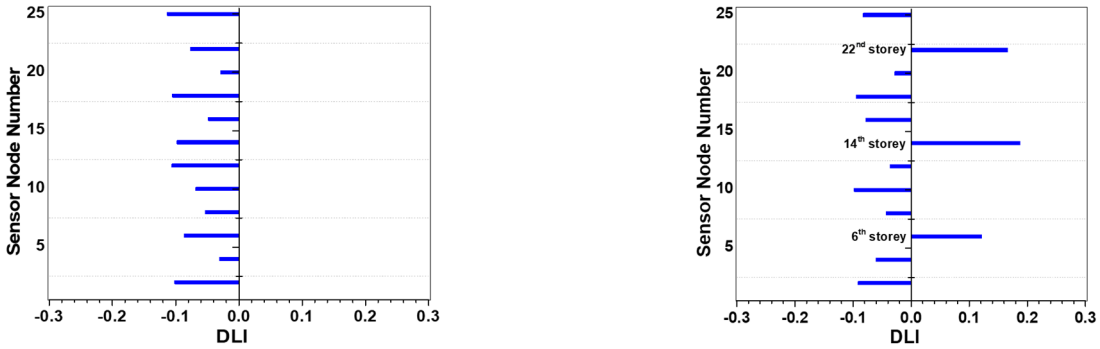

(a) 9th data-segment (b)10th data-segment

Fig. 12 DLIs for 25-storey shear building with limited (twelve) sensors placed at even storeys [2, 4, 6, 8, 10, 12, 14, 16, 18, 20, 22, 25]-2% noise

The DLIs of the 10th data-segment are shown in Fig. 11 with varying levels of noise. Figs. 11(a) and 11(b) show the presence of damage at the 6th, 14th, and 22nd stories with positive DLIs at the corresponding sensor locations. These investigations clearly show that the suggested damage diagnostic algorithm can handle EoV and detect damage locations quite precisely, despite measurement noise. The proposed algorithm's execution step, which involves processing the time history data of 25 nodes, takes 1.36 seconds to complete.

By limiting the sensors to only 12, investigations on the 25-story shear building are conducted. The optimal sensor placement (OSP) algorithm (Rao and Anandakumar 2007) recommends placing sensors at the following locations: 2, 4, 6, 8, 10, 12, 14, 16, 18, 20, 22, and 24. With these few sensors, the DLIs corresponding to the ninth and tenth data-segments are presented in Figs. 12(a) and (b), respectively. In Fig. 12(a), every DLI is negative, reflecting quite precisely the structure's damage-free state. In a similar manner, Fig. 12(b) shows sensor nodes at the 6th, 14th, and 22nd storeys have positive DLIs, indicating the presence of damage in those storeys, while the other sensor nodes have negative DLIs, reflecting a damage-free state. The results of this investigation demonstrate that the suggested damage diagnostic algorithm can operate efficiently even with a small number of sensors, negating the influence of noise and EoV.

5. Experimental investigations

5.1 Steel I-beam

The steel I beam shown in Fig. 13 is considered for the lab-level experimental investigations. The properties of a simply supported beam [ISMB 100] are

Span of the beam: 3000 mm;	Depth: 100 mm
Web thickness: 4 mm;	Flange width: 60 mm
Flange thickness: 7.2 mm;	Cross-sectional area: 1460 mm^2
Section modulus, Z_{xx}: 51.5 e03 mm^3;	Section modulus, Zyy: 10.9 e03 mm^3

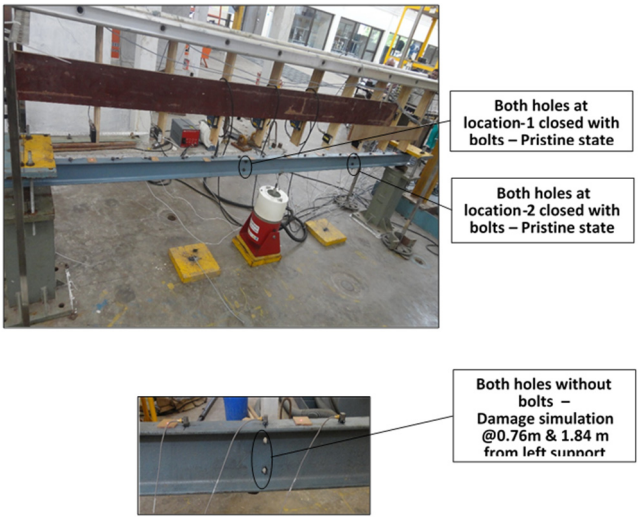

Fig. 13 Damage detection of the simply supported steel I-beam- Experimental setup

Fig. 13 presents the entire experimental setup. The instrumentation comprises 15 PZT accelerometers fixed on the beam and 15 non-contact displacement sensors placed with the wooden lever arrangement, as indicated in Fig. 13. While the acceleration data obtained from PZT sensors are used for verification of the proposed algorithm, the displacement time history measurements obtained using non-contact displacement sensors are preserved for validating other damage diagnostic algorithms. The damage is simulated by drilling holes in the web marked with circles in Fig. 13. The arrangement of accelerometers and spatial locations of damage is shown schematically in Fig. 14.

First, experiments are performed on the healthy steel beam. The holes made in the web of the beam to simulate damage are covered with bolts, as shown in Fig. 13, to simulate a healthy structure. The first four natural frequencies of the beam are found to be 36.30 Hz, 145.40 Hz, 327.50 Hz, and 579.90 Hz.

The beam is excited with random excitation using a modal shaker of 200 N sine peak force capacity, shown in Fig. 13. The test is performed in the 0–1000 Hz frequency range. Tests have been carried out using random excitations

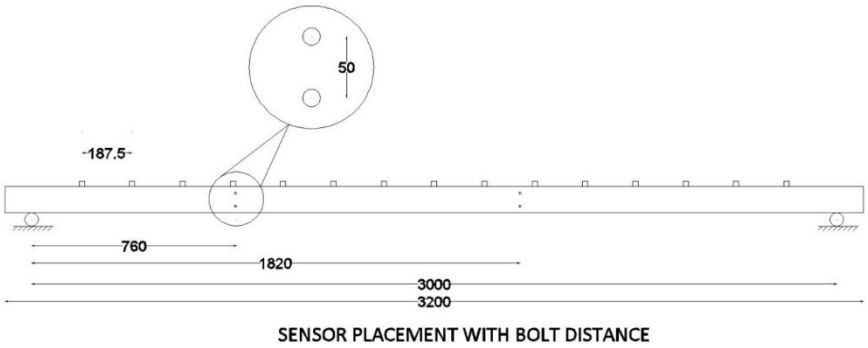

Fig. 14 Schematic diagram of experimental I-beam showing damage and sensor locations (All the dimensions indicated in the Figure are in mm)

Table 2 Test cases considered for experimental investigations with the beam model

Test case	Damage details	Number of sensors	Damage location from the left support	Number of bolts removed
Test Case-1	Single damage	15	0.76 m	Two bolts
Test Case-2	Multiple damage	15	0.76 m & 1.82 m	Four bolts
Test Case-3	Multiple damage	6	0.76 m & 1.82 m	Four bolts

to simulate operational variability. Environmental variability alters the structure's frequencies and modes. In order to simulate this scenario through lab-level experiments, small masses are placed at arbitrary locations on the beam, and their positions are changed randomly for each set of simulations. Four seconds of vibration data is collected in each experimental simulation. The sampling rate is 2400 Hz. Two hundred and fifty such independent experimental simulations are carried out on the healthy beam considering EoV. All these 250 realizations of time history data are divided into several data- segments, each with 1200 samples. These 2000 data-segments compiled from the healthy structure constitute the baseline pool. The threshold limits (THL) for each sensor location are established using the baseline pool of data.

For simulating the damage in the beam, the bolts on the web of the beam, shown in Fig. 14, at 0.76 m and 1.82 m are removed to create 8.5 mm holes. The test cases considered in the present investigations are given in Table 2. Vibration measurements of the beam in its current state with single and multiple damages as detailed in Table 2 are compiled and the current data-segments each with 1200 samples, are formed.

In order to create the current data pool and ensure that the damage occurs after 5 seconds of monitoring, ten healthy data segments from the baseline pool are added to the structure's current data-segments that correspond to both single and multiple damages. Based on the process described in the execution phase of the algorithm presented in section 3, the DLIs are computed using the current data-segments. The DLIs evaluated for the current data-segments 10 and 11 of Test Case-1 are presented in Fig. 15. All the DLIs of data-segment-10 shown in Fig. 15(a) are negative, indicating clearly that the structure is healthy. Similarly, it can be noticed from Fig. 15(b) corresponds to data-segment 11, that the DLI at sensor location 4 indicates a positive value while the remaining are negative. The damage is simulated at 0.76 m from left support, and it can be verified from Fig. 14 that the 4th sensor from Left support is the closest one to the simulated damage. TDI is worked out to

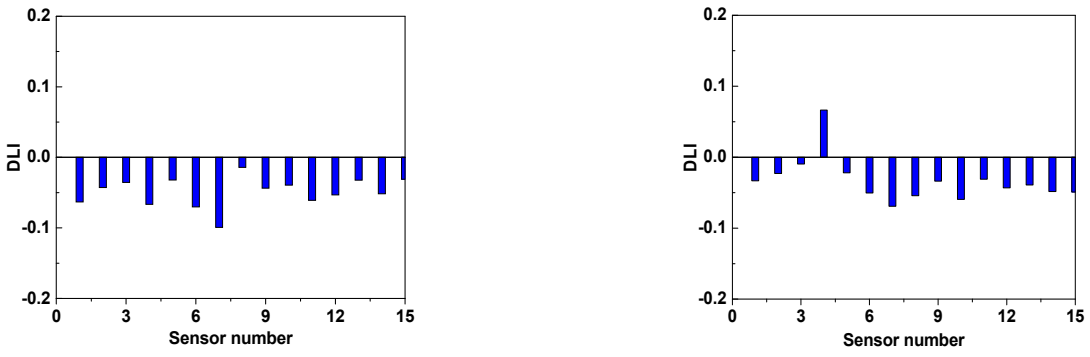

(a) 10th data-segment (b) 11th data-segment

Fig. 15 DLIs of the I-beam model: Test Case 1

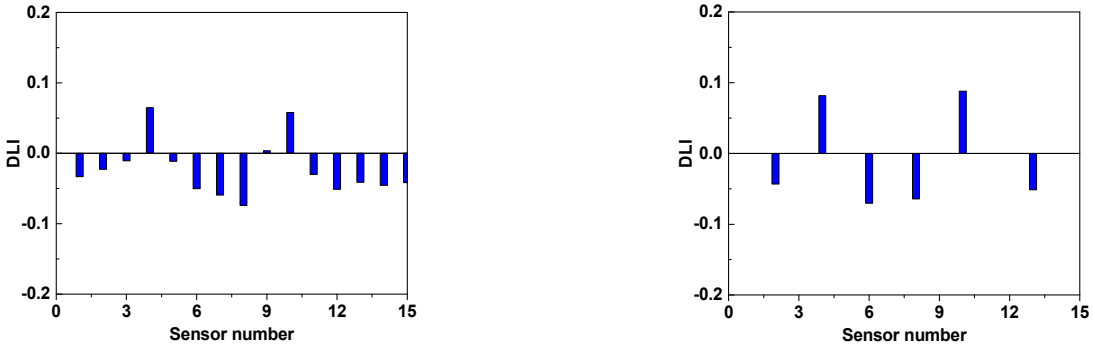

(a) 11th data-segment of Test case-2 (b) 11th data-segment of Test Case-3

Fig. 16 DLIs of the I-beam -Testcase-2 &Test case-3 (with limited sensors set [2 4, 6, 8, 10,13] placed at 0.375 m, 0.750 m, 1.125 m, 1.5 m 1.88 m, and 2.44 m from left support)

be 5.0 seconds. The DLIs are computed by the execution phase in 0.83 seconds. It involves processing the vibration measurements of 15 sensors.

Investigations are carried out along similar lines, on the I-beam with multiple simulated damages (Test case-2). The DLIs of data-segment-9 of the beam with multiple damages (Test case-2) are presented in Fig. 16(a). It can be observed from Fig. 16(a) that the DLIs corresponding to the 4th and 10th sensors are positive and the rest are negative. The multiple damages are simulated in the beam by removing the two bolts at 0.76 m and 1.82 m from the left support as shown in Fig. 14. It can be observed from Fig. 14 that sensor-4 from the left support is the closest sensor to the damage simulated at 0.76 m and similarly, 10th sensor is the closest one to the damage located at 1.82 m from the left support.

Investigations are also carried out with limited sensors, by placing only six accelerometers as dictated by the OSP algorithm (Rao and Anandakumar 2007). Accordingly, the six sensors are placed at 0.375 m, 0.75 m, 1.125 m, 1.5 m 1.88 m, and 2.44 m from the left support. Fig. 16(b) shows the DLIs evaluated with only six sensors placed on the beam. Fig. 16(b) shows positive DLIs for sensors placed at 0.75 m and 1.88 m which are in fact closer to the multiple damages present in the beam. This study proves that the proposed algorithm works even with limited sensors.

5.2 Experimental lab level ten-storey frame

The second lab experiment considered in this paper is a 10-story steel frame. Fig. 17(a) depicts the entire experimental setup. The frame is fabricated using ten numbers of steel plates of size 400 mm × 600 mm × 16 mm and four numbers of columns with dimensions 20 mm × 20 mm. All four columns and the plate at each floor level are fixed using 75 mm × 75 mm × 10 mm size L-angles, as shown in Fig. 17(b). All these column plate connections are completely welded, as shown in Fig. 17(b), to avoid torsional effects. The frame has a 300 mm clear height between any two floors. The frame is fixed over a baseplate. In order to ensure fixity at the bottom, bolts are used to secure the baseplate to the lab's rigid base floor. Natural frequencies of the structure are 5.3 Hz, 15.8 Hz, 25.9 Hz, 34.8 Hz, 44.3 Hz, 51.2 Hz, and 68.4 Hz.

Holes of size 4 mm and 8.5 mm are drilled in all the 3rd and 9th storey columns to simulate damage. Fig. 17 (c) shows a typical storey of the framed structure, with 4 mm and 8.5 mm diameter holes drilled in its columns and covered with bolts. At each floor level, biaxial accelerometers are placed for acceleration measurements along the two horizontal directions. In order to avoid torsional modal responses, accelerometers are installed at the centre of each floor (plate). A hydraulic shaker with a stringer system is used to excite the structure at the top floor with random white noise excitation to replicate ambient

(a)Experimental setup (b) Column & plate connection detail (c) Damage simulation with bolts

Fig. 17 Experimental setup for a 10-storey frame structure

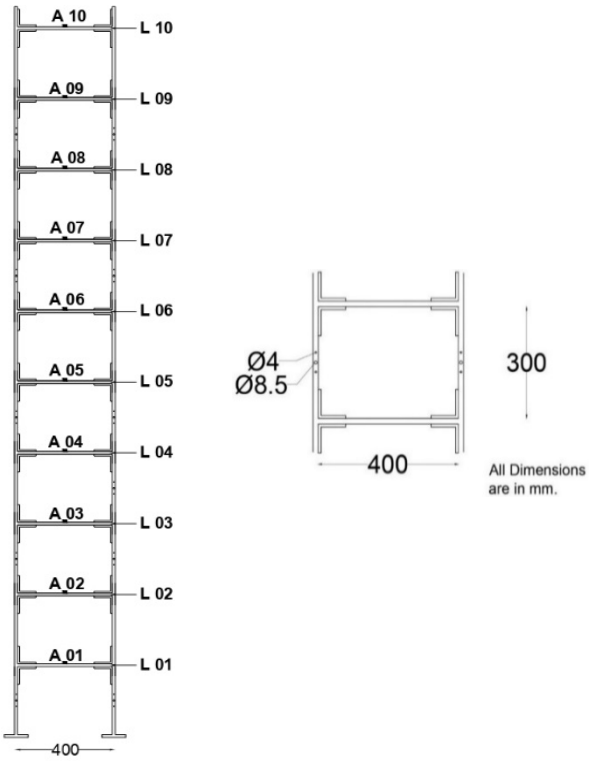

(a) (b)

Fig. 18 Schematic diagram of 10-storey steel frame: (a) accelerometers (A01-A10); (b) simulation of damage with 4 mm and 8.5 mm diameter holes on the columns

vibration. The experimental frame with the sensor locations is schematically shown in Fig. 18(a). Similarly, the schematic diagram showing the 4 mm and 8.5 mm diameter holes made in all columns of the 3rd and 9th storey for damage simulation is presented in Fig. 18(b). The 4 mm and 8.5 mm diameter holes made in the column are fitted with bolts to represent the healthy baseline scenario.

The measured vibration data of the healthy frame are compiled under varying amplitudes of random excitation. The frame is excited at the top floor using a modal shaker of 200 N sine peak force capacity, as shown in Fig. 17(a). The sampling rate is set to 2000 Hz. Since the frame structure is excited along the long-axis direction, the acceleration responses measured along the same direction are only considered in the present investigations. Once the measured healthy vibration response is collected, the baseline pool of data-segments is formed with 1000 samples in each data-segment. The threshold limits for each sensor location are established as discussed in earlier simulations.

The bolts of the columns corresponding to the 3rd storey are removed to simulate single damage in the experimental frame structure. A similar procedure is followed in compiling the vibration response of the frame structure with single damage by applying random excitation at the top floor of the frame structure and intermittently varying the excitation amplitude. A similar exercise of compiling the current acceleration time history datasets and forming data-segments of 1000 samples each is carried out by suitably partitioning the compiled current datasets of vibration response.

It is proposed to create a new set of current data-segments of the experimental framed structure to simulate a realistic situation of the structure exhibiting the presence of damage after a few seconds during online monitoring. Accordingly, new current datasets are created by suitably appending the baseline (healthy) data-segments to the current data-segments to ensure that the damage takes place during monitoring only after 6 seconds. The DLIs are evaluated with the current pool of data-segments. Fig. 19 shows the DLIs of the experimental frame structure with single damage simulated in the 3rd storey. Fig. 19(a) shows the DLIs of the 12th new current data-segment, which originally corresponded to the healthy structure, and quite rightly, all DLIs evaluated for this data-segment are found to be negative. Similarly, the DLIs of the 13th new current data-segment, shown in Fig. 19(b) exhibit positive values corresponding to the 2nd and 3rd sensors which correspond to the third storey of the frame structure. The remaining DLIs in Fig. 19(b), are negative suggesting that the rest of the structure is still healthy. The TDI is worked out to be 6 Seconds.

The bolts of all the columns corresponding to the 3rd and 9th storey are removed to simulate multiple damages in the experimental frame structure. Similar to the earlier experiment corresponding to single damage, the vibration responses are compiled, and new data-segments are formed, as discussed in the earlier section. Fig. 20 shows the DLIs evaluated using the vibration response of the frame

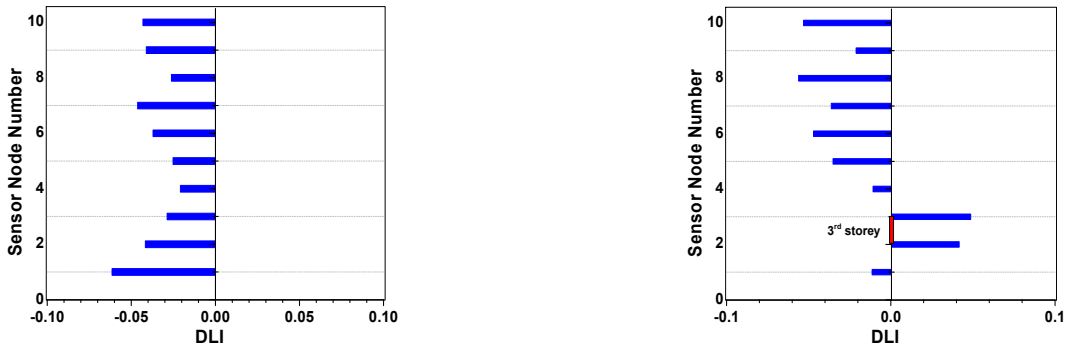

(a) 12th data-segment (b) 13thdata-segment

Fig. 19 DLIs of the ten-storey framed structure with single damage

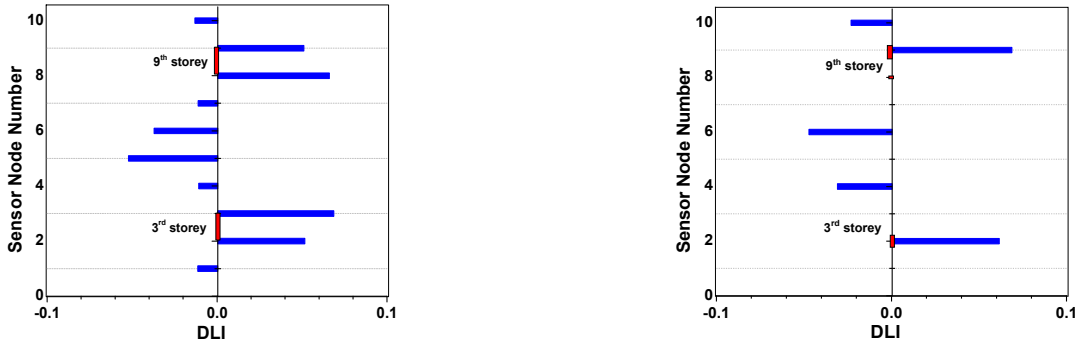

(a) 13th data-segment (b) 13th data-segment (limited sensors)

Fig. 20 DLIs of the experimental framed structure- investigations with multiple damages and limited sensors (Sensors placed on 3rd, 5th, 7th, 9th and 10th floors)

structure with multiple damages. It can be observed from Fig. 20(a) that the DLIs of the 2nd, 3rd, 8th, and 9th sensors are positive, and the remaining are negative. These positive DLIs clearly reflect damage present in the 3rd storey (2nd& 3rd sensors) and 9th storey (8th& 9th sensors). The DLIs are computed by processing the vibration data of 10 sensors in 0.64 seconds during the execution phase of the algorithm.

The DLIs evaluated with limited sensors are shown in Fig. 20(b). As suggested by the OSP algorithm (Rao and Anandakumar 2007) the sensors are placed on the third, fifth, seventh, ninth, and tenth floors. In Fig. 20(b), positive DLIs of the sensors placed at the 3rd and 9th floors indicate damage in the corresponding floors of the frame, and the remaining DLIs are negative. The diagnostic capabilities of the proposed algorithm, even with the small number of sensors, are clearly evident in this laboratory-level experimental investigation.

6. Conclusions

This paper presents a fast, real-time online damage identification and localization technique using fractal dimension theory for extracting damage features from the Degree of Scatter Waveform, DoSWF. The damage diagnostic technique discussed in this paper works with output-only measurements, doesn't need to identify natural frequencies or modal information, and doesn't even need to update FE models continuously.

Further, it is found to effectively handle EoV. Fractal dimension analysis of DoSWF is carried out to detect and localize the damage. The measured vibration responses (acceleration time history) are used to generate the DoSWF. The proposed algorithm consists of two phases. While the training phase can be performed offline, the second phase can be run online to obtain real-time information on the status of the structure's health. The proposed algorithm is evaluated initially using the synthetic vibration data obtained from the numerical simulations carried out on a simply supported beam, a twenty-five-storey shear building. Later, the measured vibration data from the lab-level experiments conducted on an I-beam and a ten-storey frame structure are used to test the algorithm for its practical amenability. The following conclusions are drawn from the studies presented in this paper.

i. Studies presented in this paper indicate that the DOS-based algorithm can identify both single and multiple structural damages.
ii. The fractal dimension analysis is an effective and faster tool for damage feature extraction from online measurements.
iii. The proposed damage localization index (DLI) is found to be effective in handling noise as well as EoV.
iv. The investigations presented in this paper demonstrate that the damage can be localized even with a small number of sensors using the proposed algorithm.
v. Extraction of damage features (DLIs) from measured vibration data is simple. Therefore, it is a handy tool for real-time diagnosis of structures through online SHM.

Acknowledgments

The research work reported in this paper is part of the mission mode project, HCP0018, funded by the Council of Scientific and Industrial Research (CSIR), India, during 2018-20. The authors gratefully acknowledge the support of the technical staff of SHM lab, CSIR-SERC, during the experimental work.

References

An, Y., Chatzi, E., Sim, S.H., Laflamme, S., Blachowski, B. and Ou, J. (2019), "Recent progress and future trends on damage identification methods for bridge structures", *Struct. Control Health Monitor.*, **26**(10), e2416. https://doi.org/10.1002/stc.2416

Avci, O., Abdeljaber, O., Kiranyaz, S., Hussein, M., Gabbouj, M. and Inman, D.J. (2021), "A review of vibration-based damage detection in civil structures: From traditional methods to Machine Learning and Deep Learning applications", *Mech. Syst. Signal Process.*, **147**, 107077. https://doi.org/10.1016/j.ymssp.2020.107077

Bernagozzi, G., Achilli, A., Betti, R., Diotallevi, P.P., Landi, L., Quqa, S. and Tronci, E.M. (2021), "On the use of multivariate

autoregressive models for vibration-based damage detection and localization", *Smart Struct. Syst.*, *Int. J.*, **27**(2), 335-350. https://doi.org/10.12989/sss.2021.27.2.335

Beygzadeh, S., Torkzadeh, P. and Salajegheh, E. (2022), "Two-stage structural damage detection method using dynamic responses based on Kalman filter and particle swarm optimization", *Struct. Eng. Mech., Int. J.*, **83**(5), 593-607. https://doi.org/10.12989/sem.2022.83.5.593

Cao, S., Guo, N. and Xu, C. (2022), "Robust damage localization in plate-type structures by using an enhanced robust principal component analysis and data fusion technique", *Mech. Syst. Signal Process.*, **162**, 108091. https://doi.org/10.1016/j.ymssp.2021.108091

Chegeni, M.H., Sharbatdar, M.K., Mahjoub, R. and Raftari, M. (2022), "New supervised learning classifiers for structural damage diagnosis using time series features from a new feature extraction technique", *Earthq. Eng. Eng. Vib.*, **21**(1), 169-191. https://doi.org/10.1007/s11803-022-2079-2

Das, S. and Roy, K. (2022), "A state-of-the-art review on FRF-based structural damage detection: Development in last two decades and way forward", *Int. J. Struct. Stabil. Dyn.*, **22**(02), 2230001.https://doi.org/10.1142/S0219455422300014

Do, N.T. and Gül, M. (2020), "A time series based damage detection method for obtaining separate mass and stiffness damage features of shear-type structures", *Eng. Struct.*, **208**, 109914. https://doi.org/10.1016/j.engstruct.2019.109914

Entezami, A., Shariatmadar, H. and Mariani, S. (2020), "Early damage assessment in large-scale structures by innovative statistical pattern recognition methods based on time series modeling and novelty detection", *Adv. Eng. Software*, **150**, 102923. https://doi.org/10.1016/j.advengsoft.2020.102923

Esteller, R., Vachtsevanos, G., Echauz, J. and Lilt, B. (1999), "A comparison of fractal dimension algorithms using synthetic and experimental data", In: *1999 IEEE International Symposium on Circuits and Systems* (*ISCAS*), Vol. 3, pp. 199-202. https://doi.org/10.1109/ISCAS.1999.778819

Guo, T., Zhang, M., Zhu, R., Zong, Y. and Pan, Z. (2022), "Vibration-based structural health monitoring using CAE-aided unsupervised deep learning", *Smart Struct. Syst., Int. J.*, **30**(6), 557-569. https://doi.org/10.12989/sss.2022.30.6.557

Hao, J., Zhu, X., Yu, Y., Zhang, C. and Li, J. (2022), "Damage localization and quantification of a truss bridge using PCA and convolutional neural network", *Smart Struct. Syst., Int. J.*, **30**(6), 673-686. https://doi.org/10.12989/sss.2022.30.6.673

Higuchi, T. (1988), "Approach to an irregular time series on the basis of the fractal theory", *Physica D: Nonlinear Phenom.*, **31**(2), 277-283. https://doi.org/10.1016/0167-2789(88)90081-4

Huang, J.Z., Li, D.S. and Li, H.N. (2023), "A new regime-switching cointegration method for structural health monitoring under changing environmental and operational conditions", *Measurement*, 212, 112682. https://doi.org/10.1016/j.measurement.2023.112682

Katunin, A., dos Santos, J.V.A. and Lopes, H. (2021), "Damage identification by wavelet analysis of modal rotation differences", *Structures*, **30**, 1-10. https://doi.org/10.1016/j.istruc.2021.01.010

Katz, M.J. (1988), "Fractals and the analysis of waveforms", *Comput. Biol. Med.*, **18**(3), 145-156. https://doi.org/10.1016/0010-4825(88)90041-8

Krishansamy, L. and Arumulla, R.M.R. (2019), "Multi constrained optimization combining ARMAX with differential search for damage assessment", *Struct. Eng. Mech., Int. J.*, **72**(6), 689-712.https://doi.org/10.12989/.2019.72.6.689

Kumar, K., Biswas, P.K. and Dhang, N. (2020), "Time series-based SHM using PCA with application to ASCE benchmark structure", *J. Civil Struct. Health Monitor.*, **10**, 899-911. https://doi.org/10.1007/s13349-020-00423-2

Lakshmi, K. (2020), "A multi-model based approach for the detection of subtle structural damage considering environmental variability", *Int. J. Struct. Stabil. Dyn.*, **20**(03), 2050038. https://doi.org/10.1142/S0219455420500388

Lakshmi, K. (2021), "Detection and quantification of damage in bridges using a hybrid algorithm with spatial filters under environmental and operational variability", *Structures*, **32**, 617-631. https://doi.org/10.1016/j.istruc.2021.03.031

Lakshmi, K. and Rama Mohan Rao, A. (2018a), "A hybrid structural health monitoring technique for detection of subtle structural damage", *Smart Struct. Syst., Int. J.*, **22**(5), 587-609. https://doi.org/10.12989/sss.2018.22.5.587

Lakshmi, K. and Rama Mohan Rao, A. (2018b), "Output-only damage localization technique using time series model", *Sādhanā*, **43**, 1-17. https://doi.org/10.1007/s12046-018-0912-0

Lakshmi, K. and Rama Mohan Rao, A. (2019), "Baseline-free hybrid diagnostic technique for detection of minor incipient damage in the structure", *J. Perform. Constr. Facil.*, **33**(2), 04019018. https://doi.org/10.1061/(ASCE)CF.1943-5509.00012

Li, H., Huang, Y., Ou, J. and Bao, Y. (2011), "Fractal dimension-based damage detection method for beams with a uniform cross-section", *Comput.-Aided Civil Infrastr. Eng.*, **26**(3), 190-206. https://doi.org/10.1111/j.1467-8667.2010.00686.x

Liu, W., Rui, E., Yuan, L., Chen, S.Y., Zheng, Y. and Ni, Y.Q. (2023), "A novel computer vision-based vibration measurement and coarse-to-fine damage assessment method for truss bridges", *Smart Struct. Syst., Int. J.*, **31**(4), 393-407. https://doi.org/10.12989/sss.2023.31.4.393

Nguyen-Ngoc, L., Tran, N. H., Bui-Tien, T., Mai-Duc, A., Abdel Wahab, M., X Nguyen, H. and De Roeck, G. (2021), "Damage detection in structures using particle swarm optimization combined with artificial neural network", *Smart Struct. Syst., Int. J.*, **28**(1), 1-12. https://doi.org/10.12989/sss.2021.28.1.001

Normant, F. and Tricot, C. (1991), "Method for evaluating the fractal dimension of curves using convex hulls", *Phys. Review A*, **43**(12), 6518. https://doi.org/10.1103/PhysRevA.43.6518

Paramanathan, P. and Uthayakumar, R. (2008), "An algorithm for computing the fractal dimension of waveforms", *Appl. Mathe. Computat.*, **195**(2), 598-603. https://doi.org/10.1016/j.amc.2007.05.011

Rama Mohan Rao, A. and Lakshmi, K. (2015), "Damage diagnostic technique combining POD with time-frequency analysis and dynamic quantum PSO", *Meccanica*, **50**, 1551-1578. https://doi.org/10.1007/s11012-015-0106-3

Rao, A.R.M. and Anandakumar, G. (2007), "Optimal placement of sensors for structural system identification and health monitoring using a hybrid swarm intelligence technique", *Smart Mater. Struct.*, **16**(6), 2658. https://doi.org/10.1088/0964-1726/16/6/071

Rao, A.R.M., Lakshmi, K. and Kumar, S.K. (2015), "Detection of delamination in laminated composites with limited measurements combining PCA and dynamic QPSO", *Adv. Eng. Software*, **86**, 85-106. https://doi.org/10.1016/j.advengsoft.2015.04.005

Sanchez, W.D., de Brito, J.V. and Avila, S.M. (2020), "Structural health monitoring using synchrosqueezed wavelet transform on IASC-ASCE benchmark phase I", *Int. J. Struct. Stabil. Dyn.*, **20**(12), 2050138. https://doi.org/10.1142/S0219455420501382

Sarmadi, H., Entezami, A., Salar, M. and De Michele, C. (2021), "Bridge health monitoring in environmental variability by new clustering and threshold estimation methods", *J. Civil Struct. Health Monitor.*, **11**, 629-644. https://doi.org/10.1007/s13349-021-00472-1

Shallan, O. and Hamdy, O. (2022), "Quantification and location damage detection of plane and space truss using residual force method and teaching-learning based optimization algorithm", *Struct. Eng. Mech., Int. J.*, **81**(2), 195-203.

https://doi.org/10.12989/sem.2022.81.2.195
Torzoni, M., Rosafalco, L., Manzoni, A., Mariani, S. and Corigliano, A. (2022), "SHM under varying environmental conditions: An approach based on model order reduction and deep learning", *Comput. Struct.*, **266**, 106790. https://doi.org/10.1016/j.compstruc.2022.106790
Wang, S.M., Jiang, G.F., Ni, Y.Q., Lu, Y., Lin, G.B., Pan, H.L., Xu, J.Q. and Hao, S. (2022), "Multiple damage detection of maglev rail joints using time-frequency spectrogram and convolutional neural network", *Smart Struct. Syst., Int. J.*, **29**(4), 625-640. https://doi.org/10.12989/sss.2022.29.4.625
Yan, A.M., Kerschen, G., De Boe, P. and Golinval, J.C. (2005), "Structural damage diagnosis under varying environmental conditions—Part I: A linear analysis", *Mech. Syst. Signal Process.*, **19**(4), 847-864. https://doi.org/10.1016/j.ymssp.2004.12.002
Zhang, G., Tang, L., Liu, Z., Zhou, L., Liu, Y., Jiang, Z., Chen, J. and Sun, S. (2021), "Enhanced features in principal component analysis with spatial and temporal windows for damage identification", *Inverse Probl. Sci. Eng.*, **29**(13), 2877-2894. https://doi.org/10.1080/17415977.2021.1954921